RSC Advances

Enhancement of the rate performance of plasma-treated platelet carbon nanofiber anode in lithium-ion battery

Journal:	*RSC Advances*
Manuscript ID	RA-ART-10-2015-020650.R1
Article Type:	Paper
Date Submitted by the Author:	08-Dec-2015

Complete List of Authors:	Han, Yu-Jin; Kyushu University, Interdisciplinary Graduated School of Engineering Sciences Lee, Choonghyeon; Seoul National University, Chemical and Biological Engineering Seo, Young Deok; Seoul National University, Chemical and Biological Engineering Nakabayashi, Koji; Kyushu University, Institute for Materials Chemistry and Engineering Miyawaki, Jin; Kyushu University, Institute for Materials Chemistry and Engineering Santamaría, Ricardo; Instituto Nacional del Carbón (INCAR-CSIC), Chemystry of Materials Menéndez, Rosa; Instituto Nacional del Carbón (INCAR-CSIC), Chemistry of Materials Jang, Jyongsik; Seoul National University, Yoon, SeongHo; Kyushu University, Institute for Materials Chemistry and Engineering

Subject area & keyword:	Electrochemical energy < Energy

Journal Name

ARTICLE

Enhancement of the rate performance of plasma-treated platelet carbon nanofiber anode in lithium-ion battery

Received 00th January 20xx,
Accepted 00th January 20xx

DOI: 10.1039/x0xx00000x

www.rsc.org/

Yu-Jin Han,[a] Choonghyeon Lee,[b] Young Deok Seo,[b] Koji Nakabayashi,[c] Jin Miyawaki,[c] Ricardo Santamaría,[d] Rosa Menéndez,[d] Jyongsik Jang*,[b] and Seong-Ho Yoon*,[a,c]

The rate performances of lithium-ion battery (LIB) anodes using platelet carbon nanofiber (PCNF) and its graphitized version (GPCNF) are enormously enhanced by introducing carbon-fluorine (C_mF_n) functional groups on the nanofiber surfaces. The C_mF_n functional groups are selectively introduced through controlled plasma treatment *in vacuo* with C_4F_8 gas. Combined X-ray photoelectron spectroscopy (XPS), Fourier transform infrared spectroscopy (FT-IR) and time-of-flight secondary ion mass spectrometry (TOF-SIMS) analyses demonstrate that the C_mF_n functional groups had mainly semi-ionic C-F bonds, which are introduced only on the surface of PCNF and GPCNF. PCNF treated with the plasma for 60 sec (PCNF-F60s) exhibits the largest discharge capacity of 387 mAh/g with increased first-cycle coulombic efficiency and a discharge capacity of 293 mAh/g at the 10C rate. These are 1.13- and 1.63-fold higher, respectively, than those of pristine PCNF. The presence of C_mF_n functional groups on the PCNF and GPCNF surfaces can reduce the resistance of the anode, which is related to lithium-ion migration and charge transfer resistance. This improved migration and reduced resistance result in a marked increase in rate performance at discharge without deterioration of the first-cycle coulombic efficiency.

1. Introduction

Large-scale lithium-ion batteries (LIBs) are increasingly found in plug-in-type hybrid vehicles (PHEVs), electric vehicles (EVs) and large-scale backup power supplies.[1] However, to successfully scale up current battery systems to meet the needs of the automotive industry, improved anode materials with better discharge rate performances and longer cycle lives are required.[2] Among the various anode materials used for LIBs, graphite has been primarily used because of its high reversible capacity, flat voltage profile, good cycle performance and relatively low cost, but it suffers from a poor rate performance.[3,4] In the graphite anode, lithium ions are converted to LiC_x with a theoretical stoichiometry of LiC_6 through intercalation of lithium ions into graphite inter-layers, resulting in an ideal discharge capacity of 372 mAh/g during de-intercalation. However, lithium intercalation/de-intercalation of graphite during the charge/discharge processes is the major cause of the low power density of the battery.[5]

Generally, the rate performance can be increased by improving electron transport pathways and shortening the solid-state diffusion paths of migrating lithium ions. This has been accomplished in graphite, for example, by using nano-structured materials.[6,7] Another effective method of improving the rate performance is via coating with metal oxides, such as SnO, ZrO_2 and Al_2O_3, on the surfaces of an anodic substrate. This increases the ion diffusivity and electronic conductivity of the overall anode.[8-12] Lee *et al.* reported that a SnO-decorated graphite anode exhibited high discharge capacity and rate capability because of uniform spreading of the SnO on the anode.[8] Recently, we reported an effective means of improving the discharge rate performance of a graphite anode by introducing meta-boric acid groups on the surface of the graphite.[12] Despite an enormous increase in the rate performance, the introduction of a metal oxide with ionic functional groups onto the surface of the graphite anode was accompanied by a large decrease in the first-cycle coulombic efficiency. To increase the rate performance without deteriorating the first-cycle coulombic efficiency, a polymer- or pitch-derived amorphous carbon coating on the graphite anode has been used. However, the fabrication process is troublesome and costly.[13,14] It remains highly desirable to develop an effective method to enhance the rate performance of the current graphite anode economically while not decreasing the first-cycle coulombic efficiency and discharge capacity.

We recently established that carbon–fluorine (C_mF_n: m = 1–3, n = 0–5) functional groups, if they were introduced only onto the surface of carbon substrates, could play a role similar to

[a] *Interdisciplinary Graduated School of Engineering Sciences, Kyushu University, Fukuoka, Japan. E-mail: yoon@cm.kyushu-u.ac.jp*
Tel.: +81-92-583-7959, Fax: +81-92-583-7879
[b] *School of Chemical and Biological Engineering, College of Engineering, Seoul National University, Seoul, Korea. E-mail: jsjang@plaza.snu.ac.kr*
Tel.: +82-2-880-7069, Fax: +82-2-888-1604
[c] *Institute for Materials Chemistry and Engineering, Kyushu University, Fukuoka, Japan*
[d] *Department of Chemistry of Materials, Instituto Nacional del Carbón, INCAR-CSIC, Oviedo, Spain*
† Electronic Supplementary Information (ESI) available. See DOI: 10.1039/c000000x/

that of ionic functional groups such as meta-boric acid. This is because the high electronegativity of fluorine atoms in the C_mF_n functional groups can facilitate fast heterogeneous electron transfer at charge and discharge. Simple plasma treatment with C_4F_8 gas *in vacuo* can introduce the C_mF_n functional groups only at the graphite surface without any covalent-type intercalation of fluorine atoms between the carbon layers. Nakajima *et al.* verified that the carbon–fluorine functional groups had different types of bonding, such as ionic, semi-ionic or covalent C–F bonds, and that their boding types induced different electrochemical behaviors of the carbon anode in LIBs.[15,16] They also showed that the bond types were dependent on the structure of the carbon material and the experimental conditions. Therefore, the carbon substrate must be chosen carefully and the optimal vacuum plasma condition identified to obtain an anodic material with improved LIB performance.

In this study, we closely investigated the effect of introducing C_mF_n functional groups on the discharge rate performance of carbon anodes in LIBs. Platelet carbon nanofiber (PCNF) and its graphitized version (GPCNF) were used as suitable model materials for this purpose because they have relatively large external surface areas, well-defined edge and basal planes and a relatively high degree of graphitization.[17] Systematic surface analyses were conducted using X-ray photoelectron spectroscopy (XPS), FT-IR spectroscopy (FT-IR) and time-of-flight secondary ion mass spectrometry (TOF-SIMS). Crystallographic and morphological properties were evaluated by X-ray diffraction (XRD), Raman spectroscopy and transmission electron microscopy (TEM). The electrochemical performance of the anode samples was evaluated by their galvanostatic charge/discharge curve, a rate capability test at high C rates, a long-term cyclability test and by electrochemical impedance spectroscopy (EIS).

2. Experimental

2.1. Preparation of PCNF and GPCNF

Platelet carbon nanofiber (PCNF) was prepared by the catalytic CVD pyrolysis of CO/H_2 gases on Fe catalyst using horizontal quartz flow reactor.[17-19] The obtained PCNF was treated with hydrochloric acid (HCl**,** 10 wt %) solution for 72 h to remove residual Fe catalyst. GPCNF was prepared by heat treatment of PCNF at 2800°C for 10 min under Ar atmosphere using horizontal type graphite furnace (Kurata Giken, Japan).

2.2. Introduction of C_mF_n functional groups on the surfaces of PCNF and GPCNF

The plasma treatment was carried out using a self-designed vacuum type plasma etcher (Korea Vacuum, Korea). The applied plasma power was 100 W and flow rate of C_4F_8 reaction gas was maintained at 5 sccm at a pressure of 200 mTorr.[20,21] The plasma treatment times were 5, 20 and 60 s. The amount of the introduced C_mF_n functional groups were controlled by plasma processing time. The C_mF_n functional group introduced onto the PCNF and GPCNF were designated as PCNF-FYs and GPCNF-FYs, respectively, where Y indicates the plasma treatment time.

2.3 Characterization

The amount of C_mF_n functional groups introduced onto the C_mF_n-modified PCNFs/GPCNFs sample was determined by elemental analysis using a CHN coder (Yanako CHN-coder MT–5, Japan) and XPS (JEOL JPS–9000MC, Mg Kα X-ray source, Japan). The atomic ratios of C, H and N atoms were determined by averaging three replica experimental values, and the F assays were defined as the difference between the sum of the contents of other elements (C, H and N) and 100%. The chemical states of the C_mF_n functional groups were determined by XPS, FT-IR and TOF-SIMS. High-resolution XPS spectra were deconvoluted and fitted using XPSPEAK41 software; a Shirley background was assumed and peaks were separated using a combination of Gaussian (80%) and Lorentzian (20%) distributions. FT-IR analysis was carried out using a Frontier FT-IR/NMR spectrometer in ATR mode with a Ge window (Perkin-Elmer, USA) from 1800 to 1000 cm^{-1} at a resolution of 4 cm^{-1}. The C and F contents of the surfaces of the C_mF_n-modified PCNF/GPCNF samples were determined by TOF-SIMS. For this analysis, PCNF/GPCNF sample powders were coated onto 1 × 1 cm^2 silicon-free tape and residual powders were removed in a nitrogen stream. For TOF-SIMS measurement, an ion TOF instrument (TOF-SIMS V, ION-TOF GmbH, Münster, Germany) in Korea Basic Science Institute (KBSI, Busan center) was used with a pulsed 30 keV Bi^+ primary beam with a current 1 pA in the positive polarity condition. The TOF-SIMS analysis area for each sample was 100 × 100 μm^2 and the data acquisition time was 100 s. Positive ion spectra were internally calibrated using H^+, H_2^+, CH_3^+, $C_2H_5^+$, $C_3H_7^+$ peaks and normalized to the respective secondary total ion yields. The chemical images of the analyzed area are recorded with 128×128 pixel resolution during the data acquisition. Charge effects are compensated by means of an interlaced pulsed electron flood gun (E_k=20 eV). The morphologies of pristine PCNF and GPCNF, and C_mF_n-modified PCNFs and GPCNFs, were observed using HR-TEM (JEM–2100F, JEOL, Japan). The crystalline properties and surface areas were evaluated using XRD (Ultima−III, Cu Kα, Rigaku, Japan), Raman spectroscopy (NRS–3000, JASCO, Japan) and nitrogen adsorption using the Brunauer−Emmett−Teller method (BET–N_2, Nippon Bell, Japan). Crystallographic analyses were performed according to a JSPS method (Gakushinho).[22] Calibration was done by mixing standard silicon powder (200 mesh, 99.99%, Soekawa Chemical Co., Japan) with each sample at 10 wt% concentration. The interlayer spacing (d_{002}) and stacking height (Lc_{002}) were calculated.

2.4. Electrochemical measurements

The electrochemical performances of the CmFn-modified PCNFs/GPCNFs were examined using a two-electrode half-cell-type CR2032 coin cell.[23] The working electrode was prepared by mixing the active material (85 wt%), styrene butadiene rubber (SBR) (10 wt%) and carboxymethyl cellulose (CMC) (5

wt%) in distilled water. The slurry was then coated onto copper foil used as the current collector and then dried at 120°C for 12 h in vacuo before passing through a roll mill under a pressure of 100 MPa. Li metal foil was used as the counter electrode. The coin cell assembly was performed in a glove box with a dew point of –88°C. The electrolyte was 1 M LiPF6 dissolved in ethylene carbonate (EC)/diethyl carbonate (DEC) (1:1 vol%, Kishida Chemicals, Japan). The assembled coin cells were charged at the rate of 0.1C, and then discharged at different rates from 0.1C to 10C between 0.003 and 1.5 V vs. Li/Li+ (TOSCAT–3100, Toyo System, Japan) to determine the rate capability (here, 1.0C = 372 mA/g) at room temperature. EIS studies were carried out by applying a small perturbation voltage of 5 mV in the frequency range from 100 kHz to 0.01 Hz at 0.2 V.[24]

3. Results and discussion

3.1. Surface characterization of the C_mF_n-modified PCNFs/GPCNFs

Fig. 1 illustrates the preparation process of the C_mF_n-modified PCNFs/GPCNFs. To synthesize the PCNF, a carbon monoxide (CO)/hydrogen (H_2) gas mixture was blown onto the active iron (Fe) catalyst in a box furnace and the carbon nanofiber having a graphene-like platelet stack was grown vertically by a catalytic reaction. After thorough washing with HCl to remove residual Fe catalyst from the PCNF, catalyst-free PCNF powder was prepared (Fig. 1a). Then the PCNF powder was graphitized in a graphitization furnace at 2800°C to produce GPCNF. The harsh graphitization condition converted the edge-abundant surface of the platelets in the PCNFs into closed dome-like loops with an enhanced graphitization level (Fig. 1c). The PCNF and GPCNF powders were then placed in the reaction chamber of a vacuum plasma etcher. When C_4F_8 gas was introduced into the chamber and the radio-frequency plasma was activated,

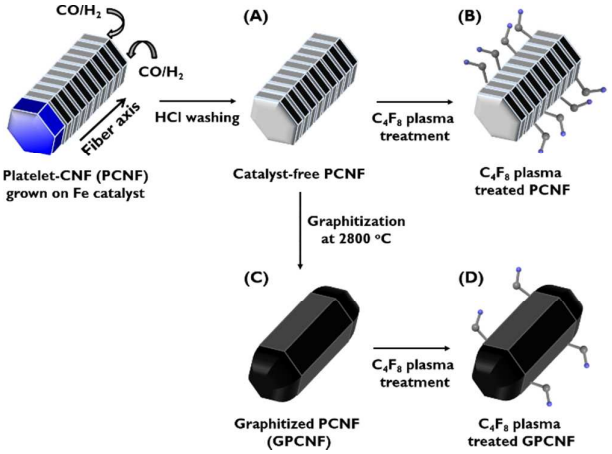

Fig. 1 Schematic presentation of the introduction of C_mF_n groups onto PCNF and GPCNF surfaces. a) Structure of pristine, catalyst-free PCNF after 72 h of washing with 10 wt% HCl; b) surface structure of PCNF after the introduction of C_mF_n groups via C_4F_8 plasma treatment; c) structure of GPCNF after graphitization of PCNF at 2800°C; d) surface structure of GPCNF after the introduction of C_mF_n groups via C_4F_8 plasma treatment. The electronegative C_mF_n groups on the surface accelerated intercalation of lithium ions during the charging process.

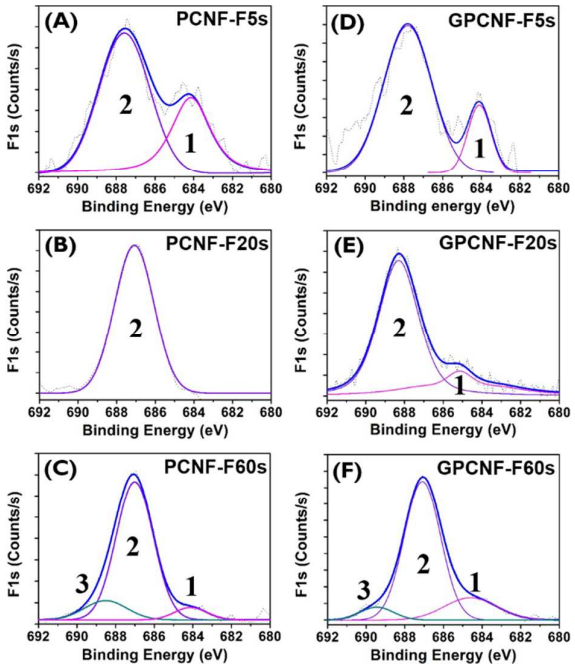

Fig. 2 Deconvoluted XPS F1s spectra. a) PCNF-F5s, b) PCNF-F20s, c) PCNF-F60s, d) GPCNF-F5s, e) GPCNF-F20s, f) GPCNF-F60s.

the C_4F_8 gas molecules were broken and the C–F fragments readily attached to the PCNF and GPCNF, forming mainly semi-ionic C_mF_n functional groups on the surface (Fig. 1b and 1d).

The elemental compositions of the C_mF_n-modified PCNFs/GPCNFs obtained by elemental analysis (EA) and XPS are summarized in Table S1. The amounts of the C_mF_n functional groups introduced on the PCNFs and GPCNFs increased as the plasma treatment time increased from 5 to 60 s. PCNF–F60s (PCNF treated with C_4F_8 plasma for 60 s) and GPCNF–F60s (GPCNF treated with C_4F_8 plasma for 60 s) showed high fluorine contents of 2.0 and 1.8% by EA analysis and 5.6 and 3.8% by XPS, respectively. The amounts of the C_mF_n functional groups evaluated by XPS were larger than those evaluated by elemental analysis. This result indicates that most of the C_mF_n functional groups were introduced on the outer surfaces of the PCNFs and GPCNFs. Furthermore, PCNF had a larger amount of C_mF_n groups than GPCNF, indicating that the edge surface of PCNF is a more active site for the introduction of the C_mF_n functional groups compared with the basal surface of GPCNF.

Fig. 2 shows the XPS F1s spectra of the C_mF_n-modified PCNFs/GPCNFs. The three different types of carbon–fluorine (C–F) bonds designated as ionic, semi-ionic and covalent were assigned as follows: Peak 1 (684 eV) ionic, Peak 2 (686–687 eV) as semi-ionic and Peak 3 (689-691 eV) as covalent.[16] In Figure 2, the most prominent C–F peak in the C_mF_n-modified PCNFs/GPCNFs spectra is that of Peak 2, indicative of semi-ionic bonding. As the plasma treatment time increased, however, Peak 3 (covalent bonding) also appeared for PCNF–F60s and GPCNF–F60s. Table S2 lists the quantitative compositions based on the deconvoluted peak area distributions of each C_mF_n functional group. The peak areas in

Table S2 also revealed that the major C–F bonding type of the C_mF_n functional groups in PCNF–F20s, PCNF–F60s, GPCNF–F20s and GPCNF–F60s was semi-ionic at 686 eV. Thus, 60 s C_4F_8 plasma treatment successfully introduced a large amount of fluorine (up to 5.6 and 3.8% for PCNF–F60s and GPCNF–F60s, respectively) on the surface, predominantly in the semi-ionic bonding state.

FT-IR and TOF-SIMS analyses were additionally conducted to further investigate the nature of the C_mF_n groups. FT-IR analyses of the C_mF_n-modified PCNFs/GPCNFs were performed between 1000 and 1800 cm^{-1} to confirm the type of C–F bonds (Fig. S1). Peaks were observed at 1127–1180 cm^{-1} and 1220–1280 cm^{-1} corresponding to semi-ionic and covalent C–F bonds, respectively (Fig. S1a and Fig. S1b). The PCNF–F60s and GPCNF–F60s absorbed more strongly at 1127–1180 cm^{-1} for semi-ionic bonding, and the peak intensity was greater for PCNF–F60s. These results indicate that the C_mF_n functional groups were more likely to be introduced at the edge surfaces of the PCNF with increasing plasma treatment time, and that the introduced C_mF_n functional groups were mainly semi-ionic. The unique semi-ionic C–F bond can exhibit different surface chemical properties from ionic or covalent bond.[25,26]

TOF-SIMS measurements were also conducted to obtain detailed chemical and molecular information concerning the C–F bonds of the C_mF_n-modified PCNFs/GPCNFs. Earlier work established that various C–F ionic species—such as CF^+, CF_2^+, CF_3^+, $C_3F_3^+$, $C_2F_4^+$ and $C_3F_5^+$—can be generated from C_4F_8 plasma processing at 100 W.[27,28] Hence, the type of C–F bond on the surface of the C_mF_n-modified PCNFs/GPCNFs needed to be verified because of the potential formation of these various ionic species through the C_4F_8 plasma processing used in this work. TOF-SIMS analysis revealed that the surface of the C_mF_n-modified PCNFs/GPCNFs contained specific C_mF_n ions, including the carbon ion C^+ (m/z of 12) and fluorine-containing functional groups such as CF_2^+ (m/z of 50), CF_3^+ (m/z of 69), $C_2F_3^+$ (m/z of 81), $C_3F_3^+$ (m/z of 93) and $C_3F_5^+$ (m/z of 131). The normalized TOF-SIMS intensity ratios for each C_mF_n ion group were also calculated to identify the major C_mF_n ion type on the C_mF_n-modified PCNFs/GPCNFs (Table S3). Normalization was performed by dividing the peak intensity of each fluorine-containing group by the peak intensity of the C^+ ion. Table S3 illustrates that the normalized peak ratios of the fluorine-containing ions increased as the plasma processing time increased. Notably, the CF_3^+/C^+ and $C_2F_3^+/C^+$ ratios for the PCNF–F60s and GPCNF–F60s were the largest among the ratios of the other samples. These results indicate that the C_4F_8 plasma treatment on the pristine PCNF and GPCNF at 100 W power successfully introduced mainly semi-ionic CF_3^+ groups and $C_2F_3^+$ groups on the surface.

3.2. Morphologies and crystalline properties of the C_mF_n-modified PCNFs/GPCNFs

High-resolution TEM (HR-TEM) images of pristine PCNF, pristine GPCNF, PCNF–F60s and GPCNF–F60s are displayed in Fig. 3. Fig. 3a clearly shows the graphitic edge planes of PCNF. The edge planes were not substantially changed even after 60 s of treatment with the C_4F_8 plasma (PCNF–F60s) (Fig. 3b).

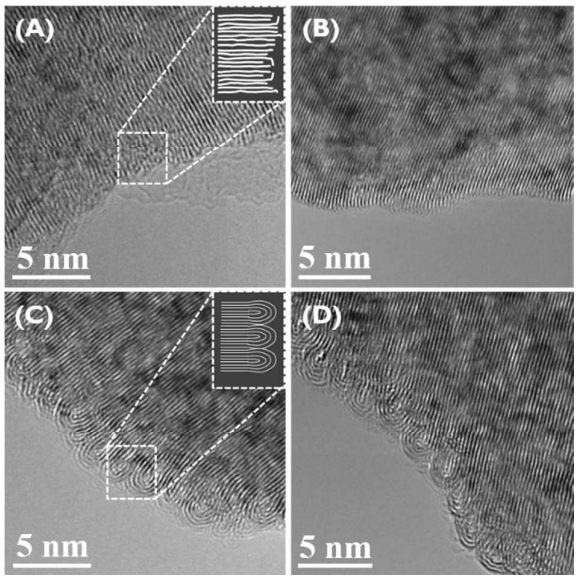

Fig. 3 TEM images of a) PCNF showing the characteristic edge-rich plane (inset: model image of the edge-rich plane); b) PCNF after 100 W C_4F_8 plasma treatment for 60 s (PCNF–F60s); c) GPCNF showing the characteristic basal-rich plane (inset: model image of the basal-rich plane); d) GPCNF after 100 W C_4F_8 plasma treatment for 60 s (GPCNF–F60s).

GPCNF, as exhibited in Fig. 3c, demonstrates dome-like closed loops of basal planes on the surface that resulted from the high temperature heat treatment (2800°C) of the PCNF precursor.[17] The plasma treatment had not altered the intrinsic surface structure of GPCNF, thus maintaining the dome-like closed loops of basal planes (Fig. 3d). The additional SEM analysis on pristine PCNF showed diameter ranging from *ca.* 100 to 300 nm, with aspect ratio of *ca.* 20 (Fig. S2a). After C_4F_8 plasma treatment for 60s, the overall morphology remained intact, with negligible change in aspect ratio of the fiber (Fig. S2b). The pristine GPCNF (displayed in Fig. S2c) also represented diameter of the fibers ranging from *ca.* 100 to 300 nm, with aspect ratio slightly decreased to 10~15. The plasma treatment also had minute impact on the diameter and length of the GPCNF (Fig. S2d).

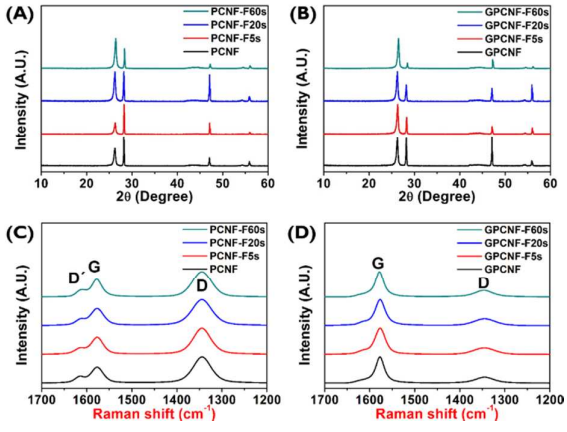

Fig. 4 XRD spectra of a) PCNF, PCNF–F5s, PCNF–F20s, PCNF–F60s and b) GPCNF, GPCNF–F5s, GPCNF–F20s, GPCNF–F60s; Raman spectra of c) PCNF, PCNF–F5s, PCNF–F20s, PCNF–F60s and d) GPCNF, GPCNF–F5s, GPCNF–F20s, GPCNF–F60s.

Details of the crystallographic and Raman characterization of the C_mF_n-modified PCNFs/GPCNFs are described in Fig. 4. In Fig. 4a and 4b, Pristine PCNF and GPCNF had relatively high degrees of graphitization, as indicated by d_{002} values of 3.367 and 3.368 Å, respectively. Lc_{002} values of 56 and 72 nm, respectively, were obtained from the XRD measurements. Fig. 4c exhibits a G peak at *ca.* 1576 cm^{-1} corresponding to the graphitic structure, and a prominent D peak at *ca.* 1350 cm^{-1} corresponding to defects in the PCNF surface. A minor D' peak at *ca.* 1620 cm^{-1} corresponding to a defective graphite structure is also present. The Raman spectra for the C_mF_n-modified GPCNFs (Fig. 4d) shows a less intense D peak and more intense G peak, with the D' peak absent because of the graphitization process. The absence of shifts in the characteristic Raman band positions indicates that the C_4F_8 plasma treatment of the PCNF and GPCNF did not substantially change their overall structures. Relatively low Raman Δν(G) values of 32.4 and 23.4 nm and R values (I_D/I_G) of 1.68 and 0.25, respectively, were measured and listed in Table S4. The unexpectedly large R value for the PCNF indicated that it had well-developed edges on the surfaces, while the d_{002} and Lc_{002} values confirmed high graphitic properties.[29]

Table S4 also shows that the d002 values of the C_mF_n-modified PCNFs/GPCNFs changed from 3.357 Å for PCNF–F5s to 3.364 Å for PCNF–F60s, and from 3.365 Å for GPCNF–F5s to 3.360 Å for GPCNF–F60s. The corresponding Lc002 values changed from 61 to 68 nm for the C_mF_n -modified PCNFs and from 73 to over 100 nm for the C_mF_n -modified GPCNFs. The values of the crystalline factors from XRD (d002 and Lc002) and Raman spectroscopy (Δν(G) and R) of the C_mF_n-modified PCNFs/GPCNFs again demonstrated that the introduced C_mF_n functional groups had a negligible impact on the crystalline properties of the PCNF and GPCNF, and that the C_mF_n functional groups were restricted to the surfaces of pristine PCNF and GPCNF by the plasma treatments. The surface areas of the pristine PCNF and GPCNF samples were 97 and 60 m2/g, respectively. The surface areas of the various C_mF_n-modified PCNFs/GPCNFs were similar; i.e., 90 to 95 m2/g for the C_mF_n-modified PCNFs and 56 to 59 m2/g for the C_mF_n-modified GPCNFs.

Based on the above combined analyses, the introduction of C_mF_n groups by plasma treatment had little effect on the morphologies and structural properties of the prepared PCNFs and GPCNFs. This was because the plasma treatment introduced those functional groups only on the surfaces of the materials without producing a covalent-type of fluorine-intercalated graphitic structure.

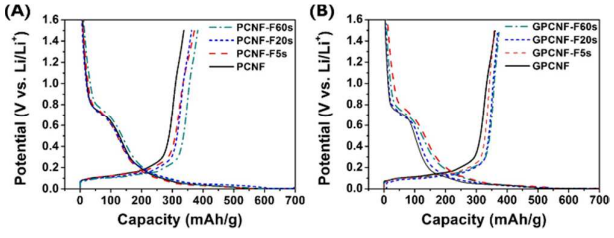

Fig. 5 Charge-discharge curves of a) PCNF, PCNF-F5s, PCNF-F20s, PCNF-F60s and b) GPCNF, GPCNF-F5s, GPCNF-F20s, GPCNF-F60s.

Table 1 Electrochemical properties of the C_mF_n-modified PCNFs/GPCNFs: Charge-discharge capacity, first-cycle coulombic efficiency, and discharge capacity and retention ratio of capacity at the 10C rate.

Samples	Charge capacity (mAh/g)	Discharge capacity (mAh/g)	First-cycle coulombic efficiency (%)	Discharge capacity at 10C (mAh/g)	Retention ratio (10C/0.1C, %)
PCNF	667	341	51	180	53
PCNF-F5s	686	370	54	210	57
PCNF-F20s	671	363	54	256	70
PCNF-F60s	692	387	56	293	76
GPCNF	663	350	52	125	36
GPCNF-F5s	680	356	52	130	37
GPCNF-F20s	682	360	53	170	47
GPCNF-F60s	681	362	53	185	51

3.3. Electrochemical performances of the C_mF_n-modified PCNFs/GPCNFs

Fig. 5 demonstrates the charge/discharge profiles of the C_mF_n-modified PCNFs/GPCNFs at the first cycle. The charge/discharge process was carried out at 0.1C between the potentials of 0.003 and 1.5 V vs. Li/Li^+. The plateau at *ca.* 0.8 V (vs. Li/Li^+) during the charge process corresponds to the reduction of the electrolyte to form a solid electrolyte interphase (SEI) on the surface of the samples. Raising the plasma processing time from 5 to 60 s increased the discharge capacities without decreasing the first-cycle coulombic efficiency. The discharge capacities of the pristine PCNF and GPCNF were 341 and 350 mAh/g, while the calculated first-cycle coulombic efficiencies were 51 and 52%, respectively (Table 1). After the plasma treatment, the C_mF_n-modified PCNFs had improved discharge capacities, increasing from 370 mAh/g for PCNF–F5s to 387 mAh/g for PCNF–F60s, with first-cycle coulombic efficiencies ranging from 54 to 56%. The C_mF_n -modified GPCNFs showed the same trend, for which the discharge capacities increased from 356 mAh/g for GPCNF–F5s to 362 mAh/g for GPCNF–F60s, and first-cycle coulombic efficiencies from 52 to 53%, respectively. Notably, the PCNF–F60s had the highest discharge capacity of 387 mAh/g and first-cycle coulombic efficiency of 56%. The improvement in discharge capacity of the C_mF_n-modified PCNFs/GPCNFs is attributed to the C_mF_n functional groups on the surface, which act as effective sites for reversible lithium ion migration at charge/discharge. Compared with the meta-boric acid group, almost 100% of the introduced C_mF_n functional groups must be effective sites because no deterioration of the first-cycle coulombic efficiency was observed.

Fig. 6 shows the discharge rate capabilities and cycle performances of the C_mF_n-modified PCNFs/GPCNFs. These materials exhibited improved rate performances up to 10C compared with pristine PCNF and GPCNF (Figure 6a). The discharge capacity at the 10C rate and the retention rate (10C/0.1C) of the discharge capacity were additionally calculated (Table 1). The C_mF_n-modified PCNFs/GPCNFs showed greatly improved discharge capacities at 10C with increasing plasma treatment time: the capacitance of 210 mAh/g for PCNF–F5s increased to 293 mAh/g for PCNF–F60s,

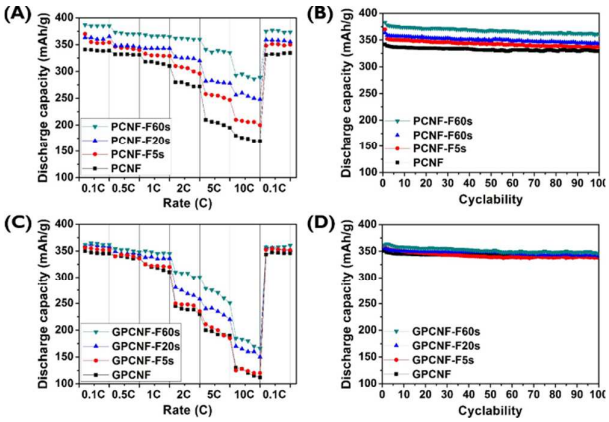

Fig. 6 Rate capability tests and cycle performances of the C_mF_n-modified PCNFs/GPCNFs: a) Rate capability tests at incremental C rates of 0.1, 0.5, 1, 2, 5 and 10C and b) cycle performances of PCNF, PCNF-F5s, PCNF-F20s, PCNF-F60s; c) Rate capability tests at incremental C rates of 0.1, 0.5, 1, 2, 5 and 10C and d) cycle performances of GPCNF, GPCNF-F5s, GPCNF-F20s, GPCNF-F60s.

while the discharge capacity of 130 mAh/g for GPCNF–F5s increased to 185 mAh/g for GPCNF–F60s. Notably, the PCNF–F60s discharge capacity was 1.63-fold greater than the 180 mAh/g measured for the pristine PCNF at the same 10C rate. As shown in Fig 6, PCNF sample showed a minute drop on discharge capacity retention (0.1C/0.1C after 10C) and maintained 97.0% of initial discharge capacity (from 341 to 331) after 10C rate. The plasma-fluorinated PCNF-F60s sample also represented maintained capacity retention rate, 96.9% after 10C rate. The retention rates (0.1C/ 10C) of the C_mF_n-modified PCNFs/GPCNFs also greatly improved; i.e., from 57 to 76% and from 37 to 51%, respectively. PCNF–F60s showed the largest value of 76% and that for GPCNF–F60s was 51%, both of which were significantly improved from the 36% for the pristine GPCNF. These outstanding characteristics can also be confirmed on the charge/discharge profiles at various current rates in Fig. S3 and 4, and Table S5. These results showed that each capacity decreased gradually with the increase of the current rates. The C_mF_n-modified PCNFs/GPCNFs exhibit a much higher capacity and higher Coulombic efficiency than that of pristine PCNFs/GPCNFs for high current rates depending on plasma treated times. From these results, we could be confirmed that high electronegativity of fluorine atoms in the C_mF_n functional groups can facilitate fast heterogeneous electron transfer at discharge. It means that the C_mF_n-modified samples have positive effect on the conductivity, thus its promising anode material for a high power battery. The C_mF_n-modified GPCNFs presented much smaller improvements in the discharge capacities and rate performances compared with the C_mF_n-modified PCNFs, possibly because of fewer electronegative C_mF_n groups being introduced onto the basal plane of the GPCNF surface during the plasma treatment process. The long-term stabilities of the C_mF_n-modified PCNFs/GPCNFs as anode materials were also evaluated. The PCNF–F60s and GPCNF–F60s anodes exhibited high capacity retention rates; i.e., 96 and 95% after 100 charge/discharge cycles, respectively. This result again

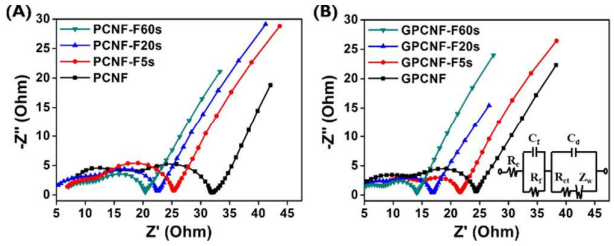

Fig. 7 EIS analysis results for a) PCNF, PCNF-F5s, PCNF-F20s, PCNF-F60s and b) GPCNF, GPCNF-F5s, GPCNF-F20s, GPCNF-F60s.

indicates that the intrinsically robust PCNF and GPCNF structures were not altered by short C_4F_8 plasma treatments and the high cyclability is attributable to the increased electrical conductivity of the semi-ionic C_mF_n groups on the anode surface.

The kinetics of the electrochemical reaction in the LIB system was studied using the Nyquist plots of the C_mF_n-modified PCNFs/GPCNFs (Fig. 7). The equivalent circuit in Fig. 7b indicates the resistance, where R_e is the electrolyte resistance, R_f represents the surface resistance due to formation of SEI and R_{ct} is the charge-transfer resistance.[30] The C_mF_n-modified PCNFs/GPCNFs had lower charge-transfer resistances than those of the pristine PCNF and GPCNF. The R_{ct} values for PCNF-F60s and GPCNF-F60s were 6.7 Ω and 4.5 Ω, respectively, lowest among the each sample series (Detailed values described in Table S6). This indicated that the charge-transfer process between the C_mF_n groups on the anode surface and the electrolyte interfaces was faster than that at the pristine PCNF/GPCNF anode–electrolyte interface. Consequently, PCNF–F60s and GPCNF–F60s had markedly lower total cell resistances.

The above results suggest that the C_mF_n functional groups introduced on the PCNF/GPCNF surfaces have two important roles: (1) they provide effective and reversible lithium-ion storage and release sites during the charge/discharge process, which increases the discharge capacity without deteriorating the first-cycle coulombic efficiency, and (2) they provide effective lithium-ion releasing gates at discharge, which increase the discharge rate performance. The semi-ionic C_mF_n groups behave quite differently from the complete ionic and covalent functional groups on the anode surface. This is because even negatively charged F-species usually act as active sites for the formation of SEI via electrolyte decomposition, which increases the irreversible capacity. On the other hand, completely covalent F-species easily form LiF irreversibly on the graphite surface, thereby decreasing the first-cycle coulombic efficiency.[16] The large electronegativity of fluorine atoms in the C_mF_n functional groups can exhibit an ionic character when lithium ions approach, and this behavior can reverse to a covalent character when lithium ions are distant from the C_mF_n functional groups. Such changes might induce acceleration of the diffusion of lithium ions in the charge/discharge process at the anode surface. Additionally, the graphitic edge planes of PCNF are more favorable sites for C_mF_n introduction. For PCNF–F60s, this resulted in a larger

increment of the discharge capacity and the rate performance while not decreasing the first-cycle coulombic efficiency.

Conclusions

In summary, the surfaces of graphitic PCNF and GPCNF nanomaterials was selectively functionalized with C_mF_n functional groups by C_4F_8 vacuum plasma treatment under controlled reaction conditions, without formation of covalent-type fluorine-intercalated graphite. The type and amount of the introduced C_mF_n functional groups on the PCNF and GPCNF depended on the intrinsic structure and the plasma treatment time. The introduction of C_mF_n functional groups was more favorable on the edge surface of the PCNF than on the basal one of the GPCNF, and increased with increasing plasma treatment time. Moreover, the introduced C_mF_n functional groups are mainly semi-ionic CF_2^+ and $C_2F_3^+$ groups, which can act as effective and reversible lithium-ion storage and release sites and as effective gates for lithium-ion release into the electrolyte solution at discharge. The C_mF_n-modified PCNFs/GPCNFs exhibited much higher discharge capacities (up to 387 and 362 mAh/g) than the pristine materials, without deterioration of the first-cycle coulombic efficiency. Furthermore, the PCNF–F60s had the greatest improvement in discharge capacity of 293 mAh/g at the high 10C rate, and an improved first-cycle coulombic efficiency of 56%. This synthesis methods using plasma treatment provide a novel technique to solve the rate performance issue for future EV and PHEV applications.

Acknowledgements

We thank Dr. J. S. Jin and Miss D. Y. Kim for helpful analyses and discussions with TOF-SIMS (ION-TOF GmbH, Ger.) in Korea Basic Science Institute (KBSI), Busan center.

Notes and references

1 B. Diouf, R. Pode, *Renew. Energ*, 2015, **76**, 375.
2 H.S. Choi, C.R. Park, *Lithium-ion Batteries*, InTech, Croatia, 2010.
3 Y. W. Cheng, C. K. Lin, Y. C. Chu, A. Abouimrane, Z. Chen, Y. Ren, C. P. Liu, Y. Tzeng, O. Auciello, *Adv Mater.*, 2014, **26**, 3724.
4 M. Gao, N. Liu, Y. Chen, Y. Guan, W. Wang, H. Zhang, F. Wang, Y. Huang, *Chem. Commun.*, 2015, **51**, 12118.
5 S. Goriparti, E. Miele, F. De Angelis, E. Di Fabrizio, R. Proietti Zaccaria C. Capiglia, *J. Power Sources*, 2014, **257**, 421.
6 T.-H. Park, J.-S. Yeo, M.-H. Seo, J. Miyawaki, I. Mochida, S.-H. Yoon, *Electrochim. Acta*, 2013, **93**, 236.
7 L. Ji, Z. Lin, M. Alcoutlabi, X. Zhang, *Energy Environ. Sci.*, 2011, **4**, 2682.
8 J. Y. Lee, R. Zhang, Z. Liu, *J. Power Sources*, 2000, **90**, 70.
9 I. R. M. Kottegoda, Y. Kadoma, H. Ikuta, Y. Uchimoto, M. Wakihara, *Electrochem. Solid-State Lett.*, 2002, **5**, A275.
10 S.-S. Kim, Y. Kadoma, H. Ikuta, Y. Uchimoto, M. Wakihara, *Electrochem. Solid-State Lett.*, 2001, **4**, A109.
11 H. Li, H. Zhou, *Chem. Commun.*, 2012, **48**, 1201.
12 J.-S. Yeo, T.-H. Park, M.-H. Seo, J. Miyawaki, I. Mochida, S.-H. Yoon, *Int. J. Electrochem. Sci.*, 2013, **8**, 1308.
13 F. S. Li, Y. S. Wu, J. Chou, M. Winter, N. L. Wu, *Adv. Mater.*, 2015, **27**, 130.
14 C. Wang, H. Zhao, J. Wang, J. Wang, P. Lv, *Ionics*, 2013, **19**, 221.
15 T. Nakajima, *Solid State Sci.*, 2007, **9**, 777.
16 T. Nakajima, *Fluorine-carbon and Fluoride-carbon Materials: Chemistry, physics, and Applications*, CRC Press, Boca Raton, USA, 2001.
17 S. Lim, S.-H. Yoon, I. Mochida, J.-h. Chi, *J. Phys. Chem. B*, 2004, **108**, 1533.
18 S.-H. Yoon, S. Lim, S.-H. Hong, W. Qiao, D. D. Whitehurst, I. Mochida, B. An, K. Yokogawa, *Carbon*, 2005, **43**, 1828.
19 T. Kim, S. Lim, K. Kwon, S.-H. Hong, W. Qiao, C. K. Rhee, S.-H. Yoon, I. Mochida, *Langmuir*, 2006, **22**, 9086.
20 S. I. Moon, J. Jang, *J Adhes. Sci. Technol.*, 2000, **14**, 493.
21 J. Jang, H. Kim, *Polym. Composite.*, 1997, **18**, 125.
22 J. S. Yeo, S. M. Jang, J. Miyawaki, B. An, I. Mochida, C. K. Rhee, S.-H. Yoon, *Nanotechnology*, 2012, **23**, 315602.
23 Y.-J. Han, J. Kim, J.-S. Yeo, J. C. An, I.-P. Hong, K. Nakabayashi, J. Miyawaki, J.-D. Jung, S.-H. Yoon, *Carbon*, 2015, **94**, 432.
24 X. Li, H. Wang, H. Song, H. Li, J. Huang, S.-H. Yoon F. Kang, *Int. J. Electrochem. Sci.*, 2012, **7**, 4397.
25 G. Panomsuwan, N. Saito, T. Ishizaki, *J. Mater. Chem. A*, 2015, **3**, 9972.
26 Y. Sato, K. Itoh, R. Hagiwara, T. Fukunaga, Y. Ito, *Carbon*, 2004, **42**, 3243.
27 I. T. Martin, E. R. Fisher, *J. Vac. Sci. Technol. A*, 2004, **22**, 2168.
28 S.-X. Zhao, Y.-R. Zhang, F. Gao, Y.-N. Wang, A. Bogaerts, *J. Appl. Phys.*, 2015, **117**, 243303.
29 A. Ramos, I. Cameán, A. B. García, *Carbon*, 2013, **59**, 2.
30 E. Barsoukov, *Impedance Spectroscopy Theory, Experiment, and Application*, John Wiley & Sons, New York, USA, 2005.

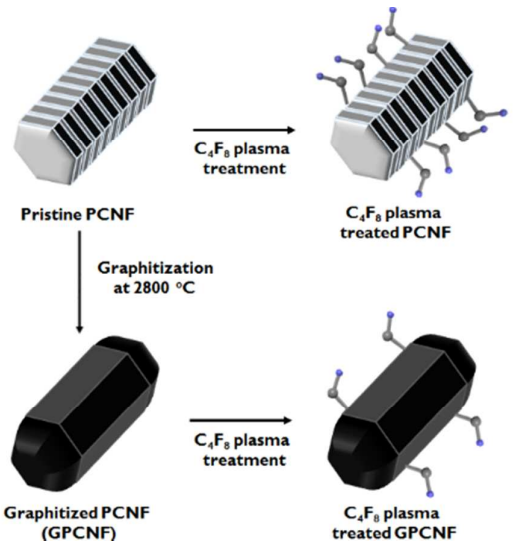

Brief C_4F_8 plasma exposure on platelet carbon nanofiber can lead to fabrication of novel LIB anodes with enhanced rate performances.